NANO LETTERS

Letter

pubs.acs.org/NanoLett

Detailed Balance Analysis and Enhancement of Open-Circuit Voltage in Single-Nanowire Solar Cells

Sunil Sandhu,[†] Zongfu Yu,[†,‡] and Shanhui Fan*[,†]

[†]Department of Electrical Engineering, Stanford University, Stanford, California 94305, United States

[‡]Department of Electrical and Computer Engineering, University of Wisconsin—Madison, Madison, Wisconsin 53706, United States

ABSTRACT: We present a detailed balance analysis of current density−voltage modeling of a single-nanowire solar cell. Our analysis takes into account intrinsic material nonidealities in order to determine the theoretical efficiency limit of the single-nanowire solar cell. The analysis only requires the nanowire's absorption cross-section over all angles, which can be readily calculated analytically. We show that the behavior of both the current and voltage is due to coherent effects that arise from resonances of the nanowire. In addition, we elucidate the physics of open-circuit voltage enhancement over bulk cells in nanowires, by showing that the enhancement is related to the removal of resonances in the immediate spectral vicinity above the bandgap.

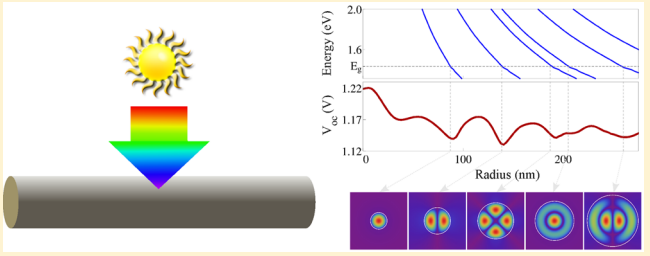

KEYWORDS: *Nanowire solar cell, detailed balance, open-circuit voltage, efficiency limit, coherent effect, resonance*

Semiconductor nanowire-based solar cells have been shown to be promising candidates for third-generation photovoltaics.[1−3] Compared with traditional thin-film solar cells,[4,5] the advantage of the nanowire cells include easily scalable manufacturing, lower cost, efficient charge separation, and tunable optical absorption.[2,3,6−11] From the optical physics point of view, the nanowire geometry is interesting in that it supports a variety of optical resonances each with a spectral peak location that directly depends on the wire's diameter.[6,12] In particular, a properly designed nanowire can support optical resonances with an absorption cross-section that is many times larger over the nanowire's geometrical cross-section.[13] Accordingly, there has been a strong interest in engineering the location of these optical resonances of the nanowire in order to enhance its optical absorption and therefore its short-circuit current performance.[6,10,11,14] However, in order to understand the fundamental limiting performance of a nanowire solar cell, these studies on the nanowire's output current behavior need to be complemented with a better understanding of the nanowire's intrinsic voltage behavior.

The intrinsic voltage behavior of a solar cell can be understood through an analysis based on the principle of detailed balance,[15,16] where one only includes the intrinsic recombination mechanisms to arrive at the limiting characteristics of a solar cell. In this letter, we carry out such a detailed balance analysis of a single nanowire solar cell, using gallium arsenide (GaAs) as an example where for recombination mechanisms we include radiative and Auger recombinations.[17] The main results of this analysis are highlighted in Figure 1. We show that an optimized single nanowire cell has a much higher open-circuit voltage as compared to that of a bulk cell. In addition, it also has a much higher short-circuit current when compared with the contributions of a region of semiconductor with the same volume located in the top surface of a bulk cell. Moreover, as one varies the wire's radius, the voltage and current show different oscillatory behaviors. Such oscillatory behaviors can be directly linked to the resonant modes of the wire and therefore are unique coherent effects arising from the wave-optical properties of the wire.

We start by first outlining the detailed balance analysis approach. This approach is generally applicable to any solar cell[15,18,19] and has been recently used to calculate the voltage behavior of a thin film GaAs cell,[20] a thin film GaAs cell with gratings,[16] and a cell with a photonic crystal top layer.[21] The starting point of this analysis is the equilibrium condition between the rates of generation and recombination of hole−electron pairs:

$$F_g - F_c(V) + R(0) - R(V) - I/q = 0 \quad (1)$$

where V is the voltage across the cell, I is the current generated by the cell, and q is the electron charge. F_g and $F_c(V)$ are the total rates of radiative hole−electron pair generation and recombination, respectively, while $R(0)$ and $R(V)$ are the total rates of nonradiative hole−electron pair generation and recombination, respectively.

In our analysis, we consider the scenario where the solar cell is at the ambient temperature T_c and is under direct sunlight. In this scenario, the total radiative generation rate is

$$F_g = F_s + F_{co} \quad (2)$$

Received: December 4, 2013
Revised: January 23, 2014
Published: January 27, 2014

   dx.doi.org/10.1021/nl404501w | *Nano Lett.* 2014, 14, 1011−1015

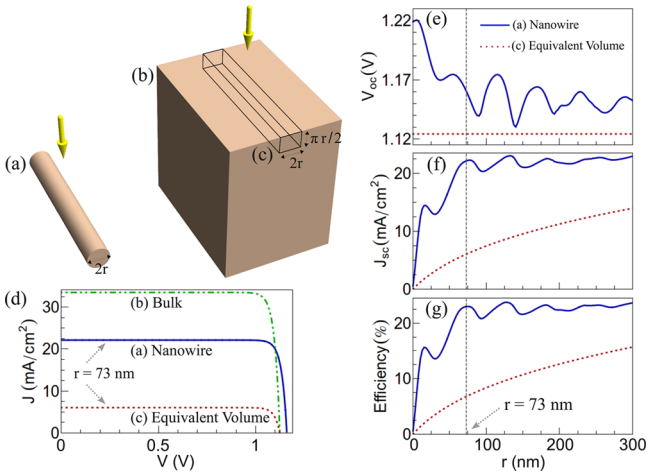

Figure 1. Comparison of current density−voltage (J−V) characteristics between a (a) GaAs single nanowire, (b) GaAs bulk structure, and (c) an equivalent rectangular volume portion (solid black line) located at the top surface of the GaAs bulk structure. The arrows indicate the direction of the incident sunlight. The plots in panel (d) are the J−V curves associated with structures (a)−(c), with radius r = 73 nm for (a) and (c). Panels (e)−(g) compare the following characteristics versus r for structures (a) and (c): (e) open-circuit voltage V_{oc}, (f) short-circuit current density J_{sc}, and (g) efficiency. The efficiency in panel (g) is defined as $\mathrm{FF}((J_{sc}V_{oc})/P_{inc}) \times 100\%$ where P_{inc} is the total incident sun radiation power per unit cell area, and FF is the cell's fill-factor.[15]

where the F_s and F_{co} are the radiative generation rate contributions due to the incoming direct sunlight and the surrounding blackbody at ambient temperature T_c, respectively. F_s is given by

$$F_s = \int_{E_g}^{\infty} dE S(E)\sigma(E, \theta = 0, \phi = 0) \tag{3}$$

where the integration is taken over all photon energies E above the cell's material bandgap energy E_g. $S(E)$ is the incident rate of solar photons per unit area per unit bandwidth at the photon energy E. We use the AM 1.5 global spectrum standard[22] for $S(E)$.

We use eq 3 for calculating the radiative generation rates of the nanowire cell and the bulk cell. In the case of the nanowire solar cell, $\sigma(E, \theta, \phi)$ is the cell's absorption cross-section spectra[13] summed over both the transverse electric (TE) and transverse magnetic (TM) incident polarizations. θ is the angle that the propagation vector of the incident light makes with the wire's longitudinal axis, while ϕ is the azimuthal angle of the propagation vector in cylindrical coordinates.

In the case of a bulk cell, $\sigma(E, \theta, \phi)$ is defined as

$$\sigma(E, \theta, \phi) = A \times a(E, \theta, \phi) \tag{4}$$

where A is the area of the cell's top surface, and $a(E, \theta, \phi)$ is the absorption coefficient spectra of the cell. θ and ϕ are the polar and azimuthal angles, respectively, that the propagation vector of the incident light makes with the top surface of the bulk cell. For a bulk cell with perfect antireflection coating, $a(E, \theta, \phi) = 1$.

In eq 2, the radiative generation rate F_{co} due to the surrounding blackbody at ambient temperature T_c is given by[23,24]

$$F_{co} = \int_0^{2\pi} d\phi \int_0^{\theta_u} d\theta \int_{E_g}^{\infty} dE \Theta(E)\sigma(E, \theta, \phi) \cos(\theta) \sin(\theta) \tag{5}$$

where $\Theta(E) = ((2E^2)/(h^3c^2))[\exp(E/(kT_c)) - 1]^{-1}$ is Planck's law[23] for the incident spectral irradiance at a temperature T_c, c is the speed of light in vacuum, and h is Planck's constant. For the integration over θ in eq 5, the upper limit θ_u is π and $\pi/2$ for the nanowire and bulk cell, respectively.

The relationship between the radiative recombination rate $F_c(V)$ in eq 1 and the voltage V across the cell is as follows:

$$F_c(V) = F_{co} \exp\left(\frac{qV}{kT_c}\right) \tag{6}$$

where k is the Boltzmann constant, and we have used Kirchoff's law[23,24] to relate the thermal equilibrium radiative emission rate of the cell to the radiative generation rate F_{co} due to the surrounding blackbody at the temperature T_c of the cell (eq 5).

The solar cell's short-circuit current I_{sc} is obtained by setting $V = 0$ in eq 1:[15]

$$I_{sc} = qF_s \tag{7}$$

By setting $I = 0$ in eq 1, the following expression is obtained from which we can solve for the open-circuit voltage V_{oc} across the cell:[15]

$$F_g + R(0) = F_c(V_{oc}) + R(V_{oc}) \tag{8}$$

For GaAs solar cells in general, the nonradiative recombination rates in eqs 1 and 8 typically include Auger recombination, the defect mediated Shockley−Read−Hall effect, and surface recombination.[25−31] Furthermore, since we want to establish a fundamental understanding of how optical physics influences the cell's performance, following ref 17 we idealize to the case of a defect-free GaAs cell with perfect surface passivation. In addition, we also assume that the cell is approximately intrinsic under illumination, resulting in a minimized Auger recombination rate that is given by[17,32,33]

$$R(V) = (C_n + C_p)Ln_i^3 \exp\left(\frac{3qV}{2kT_c}\right) \tag{9}$$

where n_i is the intrinsic carrier concentration, C_n (C_p) is the conduction-band (valence-band) Auger coefficient, and L is the thickness of the solar cell (in the case of the nanowire, $L = 2r$). In all our calculations, we consider GaAs cells operating at the ambient temperature T_c = 300 K, where[34,35] $C_n + C_p = 7 \times 10^{-30}$ cm^6·s^{-1} and $n_i = 2 \times 10^6$ cm^{-3}.

Although we do include the fundamental Auger nonradiative rate (eq 9) in all our calculations for GaAs nanowire solar cells below, we note that, for the GaAs nanowires we consider in this letter, the radiative rate dominates over this nonradiative rate. In this case, the V_{oc} in eq 8 can be approximated as follows:

$$V_{oc} \approx \frac{kT_c}{q} \log\left(\frac{F_g}{F_{co}}\right) \tag{10}$$

The validity of this approximation has also been experimentally verified for micrometer thick GaAs solar cells in ref 36. Furthermore, using this approximation, we calculate a V_{oc} of 1.12 V for a bulk GaAs cell, which is in consistency with the results in ref 20.

dx.doi.org/10.1021/nl404501w | Nano Lett. 2014, 14, 1011−1015

In addition, for all our calculations, we have neglected quantum confinement effects, which are only significant for nanowires in the radius regime $r < \sim 10$ nm.[37,38] For such ultrathin nanowires with radii below 10 nm, the Mie resonance effect is no longer prominent, and hence, the current of such cells should be small (Figure 1f). Moreover, quantum confinement effects, which further increase the effective bandgap, will further decrease the current from our calculated values here and thus further limit the efficiency. Accordingly, our analysis below will focus only on nanowires in the interesting $r > 20$ nm radii regime where the generated current is significant, and quantum confinement effects are negligible.

From eqs 1−10 we see that in order to perform a detailed balance analysis of a nanophotonic solar cell, we only have to calculate its absorption cross-section spectra $\sigma(E, \theta, \phi)$ over all angles. This absorption cross-section controls both the absorption and the emission properties of the nanophotonic cell that enters into the Shockley−Queisser's analysis.[15] Particularly, the analytical calculation of the absorption cross-section spectra of a nanowire has been well documented elsewhere,[13,39] and the only material related quantity required in this analytical calculation is the complex permittivity of GaAs as a function of photon energy. In this letter, we used the GaAs permittivity data from ref 40.

In the following, we will first present the results of the current density−voltage ($J-V$) characteristics associated with the calculated absorption cross-section for the nanowire in Figure 1a. J here is the density of current I [eq 1] in a unit length nanowire with radius r:

$$J = I/G \tag{11}$$

where G is the nanowire cross-sectional area projected onto a plane perpendicular to the direction of normally incident light:[13]

$$G = 2r \times (1 \text{ meter}) \tag{12}$$

Figure 1d compares the $J-V$ curve of an optimized nanowire with radius $r = 73$ nm (solid line), with that of a bulk GaAs cell with perfect antireflection coating (dash-dotted line). One remarkable feature of this $J-V$ curve comparison between the two structures is that the V_{oc} of the nanoscale sized wire is significantly enhanced over that of the bulk cell. This large voltage enhancement shows an important potential of the nanowire geometry for enhancing solar cell performance. Furthermore, Figure 1e shows that (i) this large voltage enhancement occurs over a wide range of radii of the nanowire and that (ii) the absolute voltage enhancement is directly dependent on the nanowire's radius.

In order to perform a volumetric comparison of the generated current density of the optimized nanowire with that of the bulk cell, Figure 1d also includes the $J-V$ curve (dotted line) associated with the contribution to the overall performance of a bulk cell from a hypothetical equivalent GaAs volume portion located at the top surface of the bulk cell (Figure 1c). This equivalent volume portion has a rectangular cross-section with a width of $2r$ and a thickness of $L = \pi r/2$. We assume that normally incident sunlight on the bulk cell undergoes single-pass absorption in the equivalent volume portion given by the following absorption coefficient in eq 4:

$$a(E, \theta = 0, \phi = 0) = 1 - \exp\left[-2\frac{E}{\hbar c}\kappa(E)L\right] \tag{13}$$

where $\kappa(E)$ is the absolute value of the material extinction coefficient at a photon energy of E,[40] and $\hbar$ is the reduced Planck constant. For voltage comparison, we directly compare the voltage of the nanowire cell with that of the bulk cell. The equivalent volume construct plays no role in the voltage comparison.

We see from Figure 1d that the current density of the nanowire is significantly enhanced over that of this equivalent volume portion. In fact, Figure 1f,g shows that the nanowire has a significant $J-V$ performance enhancement over the equivalent volume portion for a wide range of radii.

A distinctive feature of the nanowire cell is that as one varies the wire's radius, both its J_{sc} and V_{oc} oscillates (Figure 1e,f). It is important to note that the oscillation patterns of the current and voltage are different. Particularly, the radius that maximizes the J_{sc} is different from the radius that maximizes the V_{oc}. Below, we show that these behaviors are directly related to the modal nature of the structure.

External light incident on a nanowire can couple into one of the limited number of leaky mode resonances supported by the wire.[6,12] In the case of normally incident light, these leaky mode resonances can be separated into two linearly independent sets of modes, namely, transverse electric (TE) modes and transverse magnetic (TM) modes with the magnetic field and electric field, respectively, polarized along the wire's longitudinal axis. Figure 2a plots the resonant energies of the supported TE and TM modes as a function of the wire's radius for the case of normally incident light. In general, the resonant energy of each mode decreases with increasing radius of the wire. The electric field intensity profile of each mode is illustrated in Figure 2c.

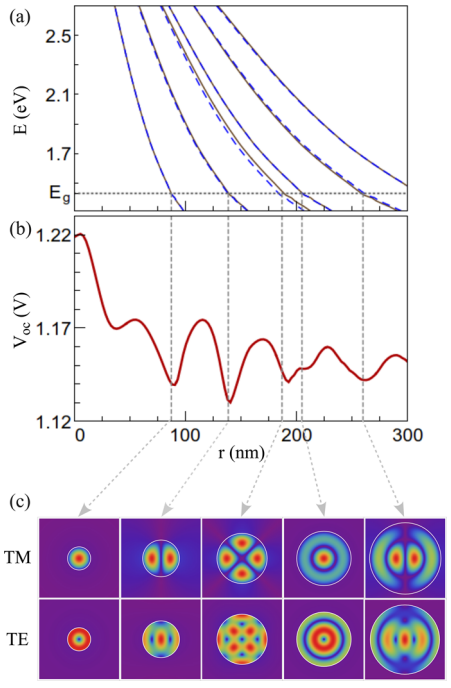

Figure 2. (a) Energies E of TM (solid line) and TE (dashed line) leaky mode resonances vs radius r of nanowire for normally incident ($\theta = 0$) light, (b) V_{oc} vs r of nanowire, and (c) TM and TE electric field across the cross-section of the nanowire around the bandgap energy E_g and at radii corresponding to the dips of the V_{oc} plot. The vertical dashed lines in panels (a),(b) show that the V_{oc} dips in panel (b) occur when there is a leaky mode resonance in the proximity of E_g.

dx.doi.org/10.1021/nl404501w | Nano Lett. 2014, 14, 1011−1015

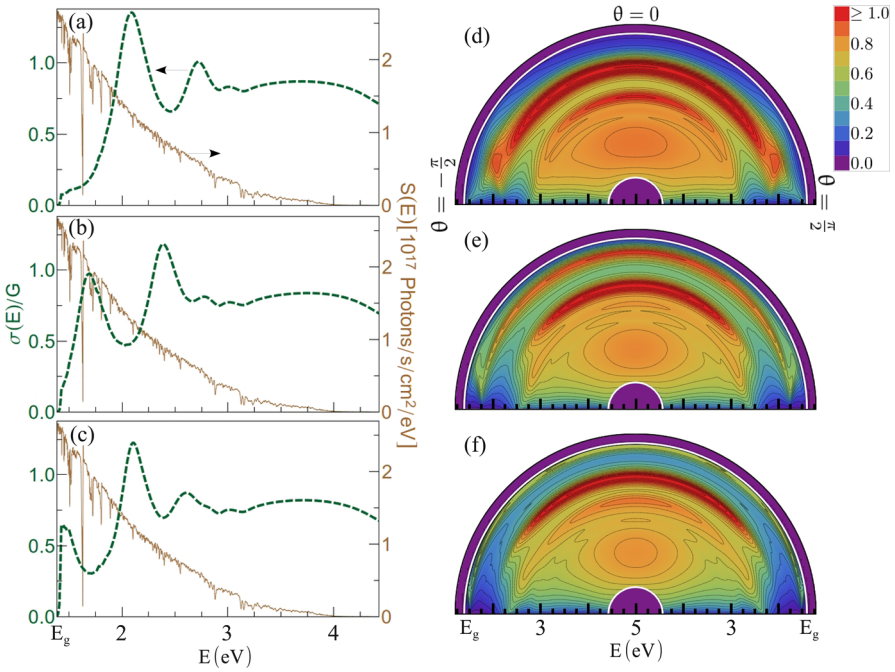

Figure 3. Dashed lines in panels (a)−(c) show the absorption efficiency $\sigma(E)/G$ as a function of photon energy E at the normal incidence angle θ = 0 for nanowires of radii: (a) r = 55.5 nm, (b) r = 73 nm, and (c) r = 88 nm. Each plot in panels (a)−(c) also includes a plot (solid line) of the Sun's incident spectral photon flux density $S(E)$ (eq 3). Panels (d)−(f) show the $\sigma(E)/G$ contour-density spectral plots at different incident angles θ for nanowires with the same radii as in panels (a)−(c), respectively. The contours in panels (d)−(f) are incremented by $\Delta\sigma(E)/G$ = 0.05. The GaAs bandgap energy E_g is located at the left boundary of panels (a)−(c). For panels (d)−(f), E_g is indicated by the outer white semicircle.

To illustrate the relation between the resonances and the J_{sc} oscillations shown in Figure 1f, the spectra (dashed lines) in Figure 3a−c show the ratios of the absorption cross-sectional area $\sigma(E)$ to the geometrical cross-sectional area G (eq 12), i.e., the absorption efficiency spectras[13] at the normal incidence angle θ = 0 for three nanowires with radii r = 55.5, 73, and 88 nm, respectively. These radii were chosen around the first J_{sc} oscillation peak at r = 73 nm.

Equations 3, 7, and 11 indicate that in order to have a large J_{sc}, the peaks of the nanowire's normal incidence absorption efficiency spectra $\sigma(E)/G$ must match well with the solar spectra $S(E)$. In order to illustrate this matching between the $\sigma(E)/G$ and $S(E)$ spectra, we have included a plot (solid line) of $S(E)$ in each of Figure 3a−c. In the range of radius between 55.5 and 88 nm, for example, the wire supports only the lowest order TE and TM modes. We see that the $\sigma(E)/G$ spectra corresponding to r = 73 nm (Figure 3b) gives the best match of its resonances with $S(E)$ since it has a strong resonance located in the lower energy side of the usable solar spectrum where the spectral component of the sunlight is stronger, resulting in the first J_{sc} peak in Figure 1f. In contrast, the position of the resonances for r = 55.5 nm (Figure 3a) and r = 88 nm (Figure 3c) are not well matched with $S(E)$ resulting in lower J_{sc} values.

However, as compared to the J_{sc} behavior above, a very different V_{oc} behavior is found in relation to the absorption efficiency spectra in Figure 3. For example, Figure 1e shows that a peak in the V_{oc} occurs at r = 55.5 nm, which is significantly different from the radius associated with the J_{sc} peak at r = 73 nm. To study the physics that controls the V_{oc} behavior in nanowires, we compare the variations, as a function of the nanowire radius, of the V_{oc} (Figure 2b) and the resonant energies E (Figure 2a). We see that each V_{oc} dip is located at a radius where there is a resonance in the immediate vicinity of the bandgap energy E_g, while each V_{oc} peak corresponds to a radius where all supported modes in Figure 2a are located away from E_g. The presence or absence of a resonance in the immediate energy range above E_g strongly influences the V_{oc} behavior. This behavior can also be seen in the $\sigma(E)/G$ spectras at all angles of incidence θ (Figure 3d−f), where the spectrum for r = 88 nm, corresponding to a V_{oc} dip, has its resonance located in the immediate vicinity of E_g (Figure 3f), whereas the other two radii, having a higher V_{oc}, have their resonances located away from E_g (Figure 3d,e).

The V_{oc} behavior of the nanowire can be understood from eqs 5 and 10. The thermal equilibrium recombination rate F_{co} [eq 5] is strongly influenced by the strength of absorption in the immediate vicinity above E_g at all angles of incidence θ. We can see this by examining the spectral integration above E_g in eq 5 that can be used to determine F_{co}. Since our nanowire cell is operating at the ambient temperature T_c and therefore satisfying $kT_c \ll E_g$, the thermal emission spectral radiance $\Theta(E)$ in the integrand of eq 5 can be approximated as

$$\Theta(E) \approx \frac{2E^2}{h^3c^2}\exp\left(-\frac{E}{kT_c}\right)H(E-E_g) \tag{14}$$

where $H(\cdot)$ is the Heaviside step function. Equation 14 shows that $\Theta(E)$ has a relatively narrow spectral width of kT_c right above E_g, and accordingly, the absorption strength in this narrow kT_c region does strongly influence the thermal emission rate F_{co} [eq 5] and therefore the cell's V_{oc} (eq 10). In contrast, this narrow kT_c width is a very small portion of the cell's total absorption bandwidth. Thus, considering the much wider bandwidth of the incoming solar radiation, we can conclude that varying the strength of absorption in this immediate vicinity above E_g has much less influence on the radiative generation rate F_s [eq 3].

dx.doi.org/10.1021/nl404501w | Nano Lett. 2014, 14, 1011−1015

We emphasize that the oscillation of both the current and the voltage as a function of radius is a coherent effect that arises from resonances of the nanowire. As the radius of the wire increases, these oscillations become far less pronounced, and the behavior of the nanowire cell approaches that of the bulk cell (Figure 1e–g). In addition, the efficiency enhancement of a nanowire over the corresponding bulk structure also vanishes in the large radius limit (Figure 1g). Hence, our work highlights the importance of optical resonances in enhancing both the current and voltage performance of nanowire solar cells. One may envision specifically tailoring these resonances to further enhance the performance of nanowire cells.

On a final note, although we specialized to GaAs nanowires in our analysis above, one may also carry out a similar detailed balance analysis on the intrinsic voltage behavior of a silicon (Si) nanowire cell. However, in a Si nanowire, strong nonradiative Auger recombination must be taken into account,[32,33] and therefore, some of the conclusions of our present work may not be straightforwardly transferred to the Si nanowire cell. We intend to address this question in future works.

AUTHOR INFORMATION

Corresponding Author

*(S.F.) E-mail: shanhui@stanford.edu.

Notes

The authors declare no competing financial interest.

ACKNOWLEDGMENTS

This work is supported by the Department of Energy Grant No. DE-FG07ER46426, by the Department of Energy Bay Area Photovoltaics Consortium (BAPVC), and by the Global Climate and Energy Project (GCEP) of Stanford University.

REFERENCES

(1) Green, M. A. *Third Generation Photovoltaics: Advanced Solar Energy Conversion*; Springer-Verlag: New York, 2003.

(2) Yan, R.; Gargas, D.; Yang, P. *Nat. Photonics* **2009**, *3*, 569–576.

(3) Li, J.; Wang, D.; LaPierre, R. R. *Advances in III-V Semiconductor Nanowires and Nanodevices*; Bentham Science Publishers: Oak Park, IL, 2011.

(4) Shah, A.; Torres, P.; Tscharner, R.; Wyrsch, N.; Keppner, H. *Science* **1999**, *285*, 692–698.

(5) Green, M. *J. Mater. Sci.: Mater. Electron.* **2007**, *18*, 15–19.

(6) Cao, L.; White, J. S.; Park, J.-S.; Schuller, J. A.; Clemens, B. M.; Brongersma, M. L. *Nat. Mater.* **2009**, *8*, 643–647.

(7) Hochbaum, A. I.; Yang, P. *Chem. Rev.* **2010**, *110*, 527–546 PMID: 19817361.

(8) Zhu, J.; Hsu, C.-M.; Yu, Z.; Fan, S.; Cui, Y. *Nano Lett.* **2010**, *10*, 1979–1984 PMID: 19891462..

(9) Garnett, E. C.; Brongersma, M. L.; Cui, Y.; McGehee, M. D. *Annu. Rev. Mater. Res.* **2011**, *41*, 269–295.

(10) Kempa, T. J.; Cahoon, J. F.; Kim, S.-K.; Day, R. W.; Bell, D. C.; Park, H.-G.; Lieber, C. M. *Proc. Natl. Acad. Sci. U.S.A.* **2012**, *109*, 1407–1412.

(11) Krogstrup, P.; Jorgensen, H. I.; Heiss, M.; Demichel, O.; Holm, J. V.; Aagesen, M.; Nygard, J.; Fontcuberta i Morral, A. *Nat. Photonics* **2013**, *7*, 1749–4885.

(12) Snyder, A. W.; Love, J. D. *Optical Waveguide Theory*, 1st ed.; Chapman and Hall: London, 1983; Chapter 24.

(13) Bohren, C. F.; Huffman, D. R. *Absorption and Scattering of Light by Small Particles*, 1st ed.; Wiley Science: New York, 1983; Chapters 3 and 8.

(14) Wallentin, J.; Anttu, N.; Asoli, D.; Huffman, M.; Åberg, I.; Magnusson, M. H.; Siefer, G.; Fuss-Kailuweit, P.; Dimroth, F.; Witzigmann, B.; Xu, H. Q.; Samuelson, L.; Deppert, K.; Borgström, M. T. *Science* **2013**, *339*, 1057–1060.

(15) Shockley, W.; Queisser, H. J. *J. Appl. Phys.* **1961**, *32*, 510–519.

(16) Sandhu, S.; Yu, Z.; Fan, S. *Opt. Express* **2013**, *21*, 1209–1217.

(17) Miller, O. D.; Yablonovitch, E.; Kurtz, S. R. *IEEE J. Photovoltaics* **2012**, *2*, 303–311.

(18) Brown, A. S.; Green, M. A. *Prog. Photovoltaics, Res. Appl.* **2002**, *10*, 299–307.

(19) Brown, A. S.; Green, M. A. *J. Appl. Phys.* **2002**, *92*, 1329–1336.

(20) Niv, A.; Gharghi, M.; Gladden, C.; Miller, O. D.; Zhang, X. *Phys. Rev. Lett.* **2012**, *109*, 138701.

(21) Munday, J. N. *J. Appl. Phys.* **2012**, *112*, 064501.

(22) NREL Air Mass 1.5 (AM1.5) Global Spectrum (ASTM173–03G), 2008; http://rredc.nrel.gov/solar/spectra/am1.5/.

(23) Landau, L. D.; Lifshitz, E. M. *Statistical Physics Part 1*, 3rd ed.; Elsevier Butterworth-Heinemann: Burlington, MA, 1980; Chapter V, p 187.

(24) Landau, L. D.; Lifshitz, E. M. *Electrodynamics of Continuous Media*, 2nd ed.; Elsevier Butterworth-Heinemann: Burlington, MA, 1993; Chapter X, p 323.

(25) Shockley, W.; Read, W. T. *Phys. Rev.* **1952**, *87*, 835–842.

(26) Hall, R. N. *Phys. Rev.* **1952**, *87*, 387–387.

(27) Sze, S. M.; Lee, M.-K. *Semiconductor Devices: Physics and Technology*, 3rd ed.; Wiley: New York, 2012; Chapter 2, p 62.

(28) Tajik, N.; Peng, Z.; Kuyanov, P.; LaPierre, R. R. *Nanotechnology* **2011**, *22*, 225402.

(29) Chang, C.-C.; Chi, C.-Y.; Yao, M.; Huang, N.; Chen, C.-C.; Theiss, J.; Bushmaker, A. W.; LaLumondiere, S.; Yeh, T.-W.; Povinelli, M. L.; Zhou, C.; Dapkus, P. D.; Cronin, S. B. *Nano Lett.* **2012**, *12*, 4484–4489.

(30) Mariani, G.; Scofield, A.; Huffaker, D. High-perfomance patterned arrays of core-shell GaAs nanopillar solar cells with in-situ ingap passivation layer. *38th IEEE Photovoltaic Specialists Conference (PVSC)*; IEEE: New York, 2012; pp 003080–003082.

(31) Huang, N.; Lin, C.; Povinelli, M. L. *J. Appl. Phys.* **2012**, *112*, 064321.

(32) Green, M. *IEEE Trans. Electron Devices* **1984**, *31*, 671–678.

(33) Tiedje, T.; Yablonovitch, E.; Cody, G. D.; Brooks, B. G. *IEEE Trans. Electron Devices* **1984**, *31*, 711–716.

(34) Pierret, R. F. *Semiconductor Fundamentals*, 2nd ed.; Prentice Hall: Upper Saddle River, NJ, 1988; Vol. *1*, Chapter 2, pp 27,31.

(35) Strauss, U.; Ruhle, W. W.; Kohler, K. *Appl. Phys. Lett.* **1993**, *62*, 55–57.

(36) Kayes, B.; Nie, H.; Twist, R.; Spruytte, S.; Reinhardt, F.; Kizilyalli, I.; Higashi, G. 27.6% conversion efficiency, a new record for single-junction solar cells under 1 sun illumination. *37th IEEE Photovoltaic Specialists Conference (PVSC)*; IEEE: New York, 2011.

(37) Duan, X.; Wang, J.; Lieber, C. M. *Appl. Phys. Lett.* **2000**, *76*, 1116–1118.

(38) Zhang, G.; Tateno, K.; Sanada, H.; Tawara, T.; Gotoh, H.; Nakano, H. *Appl. Phys. Lett.* **2009**, *95*, 123104.

(39) Wait, J. R. *Can. J. Phys.* **1955**, *33*, 189–195.

(40) Palik, E. D. *Handbook of Optical Constants of Solids*; Elsevier Academic Press: Waltham, MA, 1985; Vol. *1*, p 436.